Journal of Power Sources 182 (2008) 32–38

Contents lists available at ScienceDirect

Journal of Power Sources

journal homepage: www.elsevier.com/locate/jpowsour

Platinum–ruthenium nanoparticles in poly(2,5-dimethoxyaniline)-poly (styrene sulfonic acid) via one-step synthesis route for methanol oxidation

Li-Ming Huang, Ten-Chin Wen*

Department of Chemical Engineering, National Cheng Kung University, Tainan 70101, Taiwan

ARTICLE INFO

Article history:
Received 14 January 2008
Received in revised form 2 April 2008
Accepted 2 April 2008
Available online 10 April 2008

Keywords:
Electrocatalyst
Platinum–ruthenium nanoparticles
Poly(2,5-dimethoxyaniline)-Poly(styrene sulfonic acid)
Cyclic voltammetry
Methanol oxidation

ABSTRACT

Platinum–Ruthenium (Pt–Ru) nanoparticles were generated along with the simultaneous formation of poly(2,5-dimethoxyaniline) (PDMA) in the presence of poly(styrene sulfonic acid) (PSS) using a one-step UV-assisted method. The existence of Pt–Ru nanoparticles was verified through characterization by transmission electron microscopy (TEM), X-ray diffraction (XRD), and X-ray photoelectron spectroscopy (XPS). The latter two confirmed that the surface state of Ru in the Pt–Ru nanoparticles not only has metallic characteristics but is also present in oxidized form. The existence of PDMA in PSS was also identified using ultraviolet–visible (UV–vis) spectroscopy. Based on electrochemical measurements, PDMA–PSS–Pt–Ru exhibited a much higher electrocatalytic activity than PDMA–PSS–Pt and bulk Pt in methanol oxidation. Under the appropriate conditions, these particles can potentially serve as robust electrocatalysts in fuel cell applications.

1. Introduction

The direct methanol fuel cell (DMFC) is one of the many promising energy alternatives for the near future [1,2]. The excellent catalytic activity of Pt for methanol oxidation, especially at low temperature, makes this metal electrocatalyst attractive for use as an anode in DMFC. However, pure Pt is readily poisoned by carbon monoxide (CO), an intermediate that is produced during the electro-oxidation of methanol at low temperature. The cost of Pt-based DMFC is exceedingly high, restricting their commercial viability, because platinum is required in DMFC as on electrocatalyst.

A considerable reduction of CO poisoning has been made with the addition of other catalysts, such as Ru, Sn, W, Mo, or Os along with Pt to inhibit CO adsorption [3–5]. Among them, the Pt–Ru catalyst is the most popular for methanol oxidation in DMFC. The Pt–Ru nanoparticles can be prepared using several methods. These methods include vapor deposition, ball-milling, sol–gel, co-precipitation and, thermal decomposition [6–8]. The properties of the nanoparticles depend on the preparation method and the preparation parameters pertaining to each method. Despite progress in the scaling up of production, the cost of nanoparticle manufacturing is still relatively high [9]. Nanoparticles instability towards oxidation and agglomeration is also an issue. To achieve high dispersion for reducing the efficiency of activation, Pt–Ru catalysts are usually carried on a high-surface-area carbon support such as Vulcan XC-72. When these nanocatalysts are dispersed in carbon black, some of the active sites remain inaccessible to methanol, thus diminishing the overall reactivity of the catalyst.

There is considerable interest in wet-chemistry based on the preparation of metal nanoparticles. The versatility of this approach and its potential for the mass production of nanoparticles as catalytic materials makes it particularly attractive. Several research groups have used polymers to stabilize Pt and Pt-based alloy nanoparticles [10–13]. Niu et al. [14] studied the electrocatalytic behavior of the Pt-modified polyaniline (PANI) electrode and found that the dispersion of Pt particles into PANI is indeed more efficient than using bulk Pt for methanol oxidation. Xie et al. [15] further demonstrated that electrocatalytic activity of Pt particles can be improved appreciably by blending them into a PANI matrix containing single wall carbon nanotubes.

Thiele et al. [16] used poly(*N*-vinyl-2-pyrrolidone) (PVP) as a protecting layer after the reduction of metal ions. The protective power of PVP has been shown to be very high compared to those of other synthetic homopolymers. However, existing preparation methods of nanoparticles based on solution chemistry have a major drawback. In most cases, a solution of at least one metal precursor in the presence of a polymer is refluxed at high temperature. The temperature gradient within the solution induces inhomogeneity in the composition of the synthesized

* Corresponding author. Tel.: +886 6 2385487; fax: +886 6 2344496.
E-mail address: tcwen@mail.ncku.edu.tw (T.-C. Wen).

0378-7753/$ – see front matter © 2008 Elsevier B.V. All rights reserved.
doi:10.1016/j.jpowsour.2008.04.006

nanocrystals when convection heating is used. The presence of such temperature gradients may lead to a broad distribution of particle size. We are currently developing a new synthesis procedure for generating silver (Ag) nanoparticles in a simultaneously formed conducting polymer matrix [17,18]. A composite consisting of poly(2,5-dimethoxyaniline) (PDMA), poly(styrene sulfonic acid) (PSS), and Ag nanoparticles exhibited a few significant features. PDMA was chosen as the polymer matrix because it is soluble in common organic solvents, and has conductivity similar to that of PANI, but processes different redox characteristics [19–21]. In addition, the low oxidation potential of PDMA further aids in the formation of the nanoparticles from their metal precursor ions.

In light of our previous work [17,18], we proposed a novel and easy way to synthesize Pt–Ru nanoparticles in a PDMA–PSS matrix. The strategy involves the simultaneous formation of PDMA and Pt–Ru nanoparticles in the presence of PSS. The synthesis utilizes the in situ generation of a nanoreactor for the formation of alloy nanoparticles. The first step involves the self-assembling of DMA molecules through non-covalent binding between amine nitrogen and sulfonic groups in PSS. Upon UV illumination on the metal precursor $H_2PtCl_6/RuCl_3$ solution in the DMA–PSS matrix, Pt^{4+}/Ru^{3+} ions oxidate DMA and produce DMA radical cations, leading to the polymerization of DMA with its monomers attached to the PSS backbone. The amine nitrogens of PDMA act as sites for reducing the Pt^{4+}/Ru^{3+} ions. Consequently, the amine sites of PDMA can transform into imine units (resulting in the emeraldine state), and Pt/Ru particles can be formed in the nanoreactor. Because PDMA is mostly bound to PSS, the sulfonic acid groups of PSS and emeraldine units of PDMA can act as nuclei for the formation of Pt/Ru particles in the PDMA–PSS nanoreactor. In addition, because PDMA has a low oxidation potential, the formation of alloy nanoparticles through the reduction of Pt and Ru ions can be facilitated by UV illumination. Pt–Ru nanoparticles can be directly lodged in the PANI–PSS matrix without any additional binder on the current collector. PDMA acts as an electronic conductor and shuttles the electrons through the Pt–Ru electrocatalyst during methanol oxidation. Also, sulfonic acid groups of PSS furnish a pathway for transporting protonic species. The above are all advantages of using these particles in DMFC applications.

2. Experimental

2.1. Reagents

Reagent-grade DMA (Fluka) and PSS (molecular weight = 75,000, Aldrich) were used to prepare the polymer matrix. H_2PtCl_6 (Premion) and $RuCl_3$ (Johnson Mattey) were used as the metal precursors. HCl (Merck) and methanol (Merck) were used as received.

2.2. Synthesis of PDMA–PSS–Pt–Ru nanocomposite

PDMA–PSS–Pt–Ru nanocomposite was prepared by the simultaneous polymerization of DMA and a reduction of Pt^{4+} and Ru^{3+} ions in the PSS medium by the illumination of a layer of a solution containing DMA and the PSS of Pt^{4+} and Ru^{3+} ions over cleaned indium tin oxide (denoted as ITO, 1.0 cm × 1.0 cm). Before each experiment, ITO coated glass was cleaned in an ultrasonic bath using double distilled water and isopropanal, then dried with moisture-free nitrogen flow, followed by UV-O_3 treatment for 20 min.

A typical procedure is outlined below. Two solutions, "A" and "B", were prepared separately. Solution A was prepared by dissolving 0.19 g (25 mM) DMA in 50 mL (2 mM) PSS solution. Solution "B" was prepared by adding 46.1 mL H_2PtCl_6 (5 mM) and 3.9 mL $RuCl_3$ (15 mM) to a 50 mL solution containing 0.01 M HCl and 0.1 M KCl. Solutions "A" and "B" were then mixed and sonicated for 10 min. A dose of 45 μL of the mixed solution was dropped on a clean ITO substrate (1.0 cm × 1.0 cm) and illuminated by UV radiation (254 nm) for 2 h. The PDMA–PSS–Pt–Ru nanocomposite then formed on the ITO substrate.

2.3. Characterization

Ultraviolet–visible (UV–vis) spectra of the PDMA–PSS–Pt–Ru nanocomposites were recorded by a Shimadzu UV-2100 UV–vis spectrophotometer. TEM characterization was made on a JEOL model 1200-EX instrument operated at a voltage of 120 kV. The samples for TEM analysis were prepared by placing the PDMA–PSS–Pt–Ru nanocomposite solution onto a carbon-coated copper grid. After evaporating the sample drops for one day, the excess solution was removed with blotting paper. X-ray diffraction (XRD) patterns of the PDMA–PSS–Pt–Ru nanocomposite were collected by exposing the sample to Siemens D5000-X-ray source with Cu Kα (1.542 Å). The spectra were scanned in the range $2\theta = 38–90^\circ$. The XPS measurements were carried out using ESCA 210 and Microlab 310 D (VG Scientific, Ltd., United Kingdom) spectrometers. XPS spectra were recorded with Mg Kα ($h\nu = 1256.6$ eV) irradiation, whose photon source was driven by 12 kV and an emission current of 20 mA. The pressure in the base chamber of the spectrometer was kept at approximately 10^{-10} mbar during the measurements.

Electrochemical characterization of the catalyst was performed using a PGSTAT20 electrochemical analyzer, AUTOLAB Electrochemical Instrument (The Netherlands). All the experiments were carried out in a three-component cell in which an ITO coated glass plate (1 cm^2 area), Ag/AgCl (in 3 M KCl), and platinum wire were used as working, reference, and counter electrodes, respectively. A Luggin capillary, whose tip was set at a distance of 1–2 mm from the surface of the working electrode, was used to minimize the potential drop across electrolyte solutions.

3. Results and discussion

3.1. Characterization of PDMA–PSS–Pt–Ru nanocomposite

Following our previous work [17,18], a novel and easy way is developed to prepare Pt–Ru electrocatalysts in PDMA–PSS matrix. It has been reported that a wide range of chemical oxidations, such as $(NH)_4S_2O_8$, H_2O_2, $K_2Cr_2O_7$, and $FeCl_3$, were successfully employed for the polymerization of ANI. The formation of a polymer is favored by the fact that the oxidation potential of a monomer is compatible with the reduction potential of oxidants. The electron-donating methoxy groups in the aromatic ring can provide a suitable environment for the Pt/Pt–Ru ions through the amine groups in PDMA. The low oxidation potential of PDMA is beneficial for the formation of Pt/Pt–Ru nanoparticles from Pt^{4+}/Ru^{3+} ions:

$$\text{PDMA} \rightarrow \text{PDMA}^{n+} + ne^-, E_{\text{PDMA}} < 0.607\ \text{V vs. NHE}$$

$$Pt^{4+} + 4e^- \rightarrow Pt, E_0 = 0.735\ \text{V vs. NHE}$$

$$Ru^{3+} + 3e^- \rightarrow Ru, E_0 = 0.662\ \text{V vs. NHE}$$

UV illumination facilitates the quick formation of polymers and Pt/Ru. Photons make the DMA monomer excited, making it more reactive. At the early stage of the polymerization, this accelerates the initiation of the polymerization by promoting the formation of DMA radical cations, favoring the nucleation of Pt/Ru and the propagation of PDMA.

Prior to the polymerization, the DMA–PSS complex is first formed. DMA molecules are bound to PSS through the interactions between SO_3H groups in PSS and NH_2 groups in DMA. Two methoxy groups in DMA push electrons to the aromatic ring, facilitating the delocalization of electrons to nitrogen atoms. The nanoreactor for the formation of Pt–Ru electrocatalyst was generated through the self-assembly of DMA with PSS and subsequent polymerization. Simultaneously, Pt^{4+} and Ru^{3+} ions undergo reduction by extracting electrons from the nitrogen atom in NH_2 groups of DMA. Thus, Pt–Ru alloy nanoparticles easily form upon the addition of Pt^{4+} and Ru^{3+} ions to the DMA–PSS solution. UV illumination excites the non-bonding electrons in nitrogen atoms and generates DMA radical cations. The radical cations further proceed in the polymerization to yield PDMA. Meanwhile, Pt–Ru particles are formed within natural nanoreactors created by the PDMA–PSS matrix. The PDMA–PSS matrix prevents aggregation of Pt–Ru particles. The characterization results of the catalyst composite as analyzed by TEM, UV–vis, XRD and XPS are presented below.

The qualitative and selective TEM images of PDMA–PSS, Pt, and Pt–Ru nanoparticles in the PDMA–PSS matrix are shown in Fig. 1. The wires of PDMA–PSS (Fig. 1a) are linked by many "cross-linking points" and porous networks. The wire diameter in the PDMA–PSS three-dimensional networks is about 60 nm. As shown in Fig. 1b and c, Pt and Pt–Ru nanoparticles are embedded in the PDMA–PSS matrix, in which the former has black spots and the latter has a gray network structure. The sizes of Pt and Pt–Ru nanoparticles are 8 and 4 nm, respectively, as estimated by averaging the sizes from 100 randomly selected particles. In the same deposition area, loading of Pt particles (6.44%, from XPS results) in the PDMA–PSS–Pt is slightly larger than that in the PDMA–PSS–Pt–Ru (6.22%). The different loading of Pt particles might affect the density of Pt and Pt–Ru nanoparticles in PDMA–PSS matrix. In the selective TEM images, the dispersion of Pt nanoparticles seems to be better than that of Pt–Ru nanoparticles in the PDMA–PSS matrix. However, a closer inspection reveals that Pt particles appeared in the forming of agglomerates in PDMA–PSS. Individual small Pt–Ru nanoparticles (4 nm) can be observed for PDMA–PSS–Pt–Ru. The TEM results suggest that the addition of Ru reduces the catalyst particle size, as previously observed in carbon-supported Pt–Ru vs. carbon-supported Pt catalyst systems [22]. The effects on the catalyst particle size are expected to be beneficial in the case of Ru addition, as the surface area per mass of catalyst increases upon Ru addition.

The UV–vis spectra of PDMA–PSS, PDMA–PSS–metal composites, and oxidant solutions (H_2PtCl_6 and $RuCl_3$) are shown in Fig. 2. Two peaks at 328 and 470 nm, a shoulder around 592 nm, and a broad peak beyond 760 nm were observed for PDMA–PSS and PDMA–PSS–metal composites. The absorption peaks at 328 and 470 nm are attributed, respectively, to the π–π^* transition and polaronic transitions of the doped and protonated PDMA. The peak around 592 nm signifies the doping of PDMA by sulfonic acid groups in PSS. The broad peak around 760 nm corresponds to the π-polaron transition of PDMA [17,23–25]. The oxidants, $PtCl_6^{2-}$ and Ru^{3+}, have absorption peaks at 266 and 210 nm, respectively (curves d and e, inset). After UV irradiation of the solution containing $PtCl_6^{2-}$ and Ru^{3+} ions and DMA in PSS for 2 h, UV–vis spectra show the formation of PDMA (curves b and c) as compared to the existence of corresponding bands of PDMA. The decrease in absorbance values of the peaks of $PtCl_6^{2-}$ and Ru^{3+} is attributed to the simultaneous formation of Pt–Ru particles along with PDMA. It should be noted that the π–π^* absorption of PDMA caused a decrease in the absorbance and shifted it to 338 and 344 nm upon the formation of PDMA–PSS–Pt or PDMA–SS–Pt–Ru composites. In the present work, the estimated particle sizes of Pt and Pt–Ru nanoparticles are 8 and 4 nm, respectively. Pt nanoparticles in PDMA–PSS may

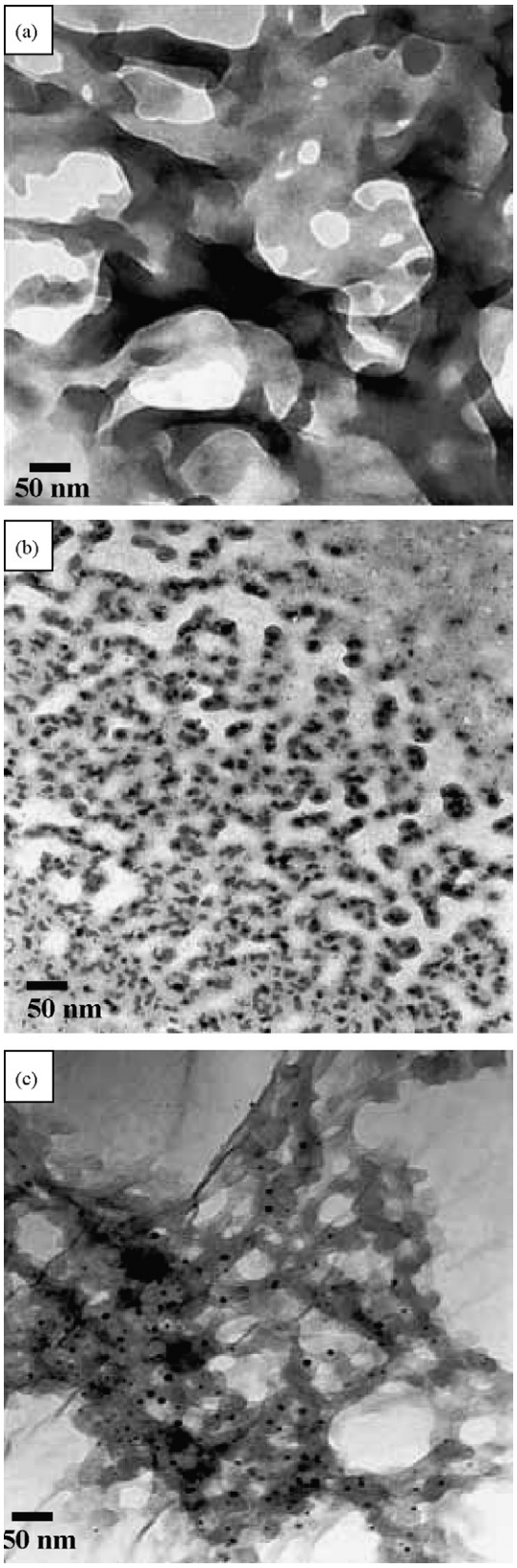

Fig. 1. TEM images of (a) PDMA–PSS, (b) PDMA–PSS–Pt, and (c) PDMA–PSS–Pt–Ru composites.

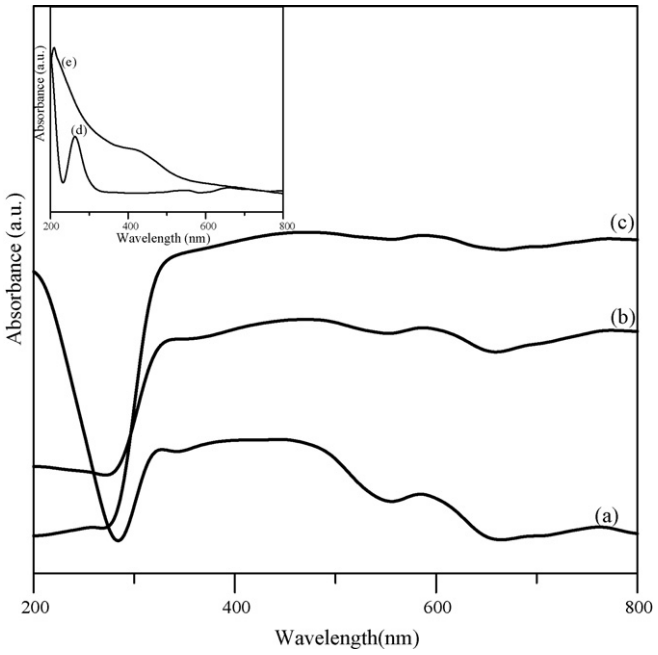

Fig. 2. UV–vis spectra of (a) PDMA–PSS, (b) PDMA–PSS–Pt and (c) PDMA–PSS–Pt–Ru composites. The insets are: (d) H_2PtCl_6 precursor and (e) $RuCl_3$ precursor solutions.

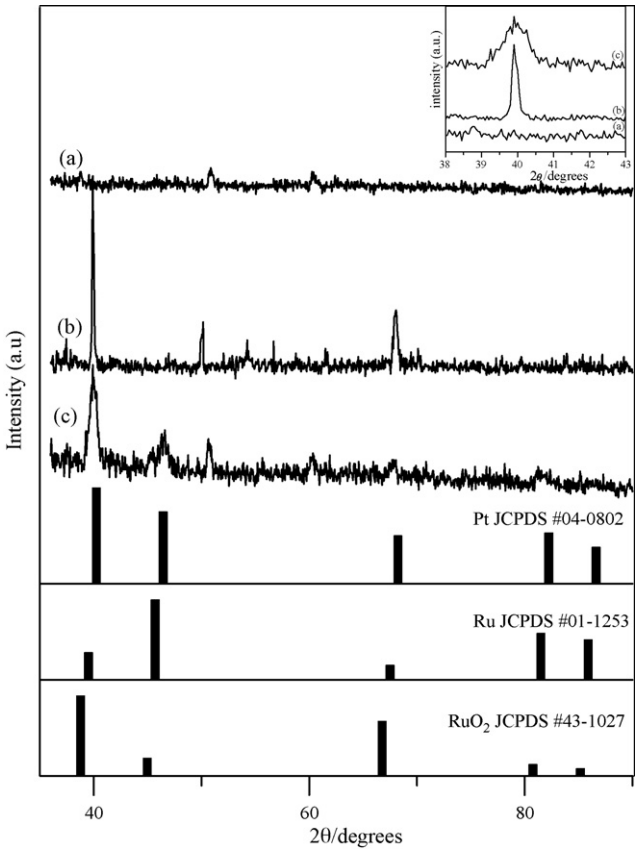

Fig. 3. X-ray diffraction patterns of (a) PDMA–PSS, (b) PDMA–PSS–Pt and (c) PDMA–PSS–Pt–Ru nanocomposites. The inset is the X-ray diffraction patterns in the range of 38–42°.

have a different environment (bound to protonated imine sites) compared to the Pt–Ru nanoparticles in PDMA–PSS. The interaction between the quinoid rings (imine) of PDMA and Pt nanoparticles is different from that between PDMA and Pt–Ru nanoparticles due to the different particle sizes (quantum size effects) of Pt and Pt–Ru [26,27]. Therefore, different interactions between the quinoid rings of PDMA and Pt/Pt–Ru nanoparticles result in the band shift of the π–π^* absorption for PDMA–PSS–Pt and PDMA–PSS–Pt–Ru.

Representative XRD results are shown in Fig. 3. Curve a exhibited a weak and broad peak, indicating that PDMA–PSS was almost amorphous. The diffraction peaks at 39.6°, 46.2°, and 67.8° can be observed for PDMA–PSS–Pt and PDMA–PSS–Pt–Ru composites. These peaks correspond to (1 1 1), (2 0 0) and (2 2 0) reflections of face-centered cubic (f.c.c.) crystal lattice of Pt. XRD patterns for PDMA–PSS–Pt and PDMA–PSS–Pt–Ru closely reflect the referenced patterns of Pt and Pt–Ru despite their shifts in the 2θ values compared to those of the pure f.c.c. structure of Pt. This observation is consistent with those of other researchers [28,29]. Note that there are no distinct peaks related to tetragonal RuO_2 or hexagonal close-packed (h.c.p.) Ru phases when Ru is added to PDMA–PSS. The lack of Ru diffraction peaks can be partly assigned to the fact that some of the Ru is incorporated into the face-centred cubic Pt lattice, as well as the fact that intensities of the Ru diffraction peaks are very weak. The inset of Fig. 3 shows an enlarged view of Pt (1 1 1) diffraction peaks for PDMA–PSS, PDMA–PSS–Pt, and PDMA–PSS–Pt–Ru. The (1 1 1) diffraction peaks of Pt in PDMA–PSS–Pt–Ru composite became broad compared to those of PDMA–PSS–Pt, which is attributable to strong interparticle interactions between Pt and Ru nanoparticles. This result is consistent with previous studies on Pt–Ru which showed that Pt f.c.c. peaks appeared in XRD spectra only in Pt–Ru alloys containing Ru up to 52 wt% [30,31]. The average particle size of Pt–Ru nanoparticles was ca. 4 nm from XRD peaks, as calculated using the Debye–Scherrer equation $Dc = 0.9\lambda/\beta\cos\theta$ (where λ is the X-ray wavelength, 1.5406 Å, β is the full width at half maximum of the radius)[32], in agreement with the average size of 4 nm observed in the TEM images.

The XPS spectrum of core-level N_{1s} for PDMA–PSS–Pt–Ru is shown in Fig. 4a. When the multiple peaks were deconvoluted into Gaussian component peaks [33], we component peaks at 396.6, 399.3, 401.6 and 402.4 eV, corresponding to —N═, —N–, —N^+, and ═N^+, respectively. Integrating the areas under these peaks, the ratios of these components are 0.35, 0.37, 0.25 and 0.03. The area ratio of [—N═]/[—N—] is almost 1.0, favoring the presence of the emeraldine type structure for PDMA in the PDMA–PSS–Pt–Ru composite.

Another important feature is the high positive charge nitrogen (0.28) in PDMA–PSS–Pt–Ru. This indicates that PDMA in PDMA–PSS–Pt–Ru is in the doped state due to doping from sulfonic acid groups in PSS. This observation implies that electrons might be easily conveyed through the conjugated polymer matrix to the current collector during methanol oxidation. Fig. 4b exhibits two peaks, one belonging to low energy band ($4f_{7/2}$) at 71.7 eV and the other to a high-energy band ($4f_{5/2}$) at 3.6 eV or higher, suggesting that there must exist two different Pt entities in the composite because of chemical nonequivalent metal or ligand sites on surfaces as shown in previous studies [34]. The two broad bands were deconvoluted into two pairs of Pt_{4f} peaks at 71.6, 74.9 (Pt(0)) and at 72.8, 75.8 eV (Pt(IV)), with the corresponding area ratios of 0.83 and 0.17.

The existence of Pt(IV) in the PDMA–PSS–Pt–Ru composite can be explained by the complexation of Pt ions with amine groups in PDMA–PSS–Pt–Ru or due to the incomplete reduction reactions of Pt ions. Similar electrostatic interactions between Pt ions and amine groups have been identified in other studies on salt loaded dendrimer-polymer networks with amine groups [35]. Fig. 4c shows the narrow scan Ru_{3p} core-level XPS spectrum of PDMA–PSS–Pt–Ru. The Ru_{3p} spectrum, used instead of the Ru_{3d} spectrum to avoid the interference of the C1s signal, can be decon-

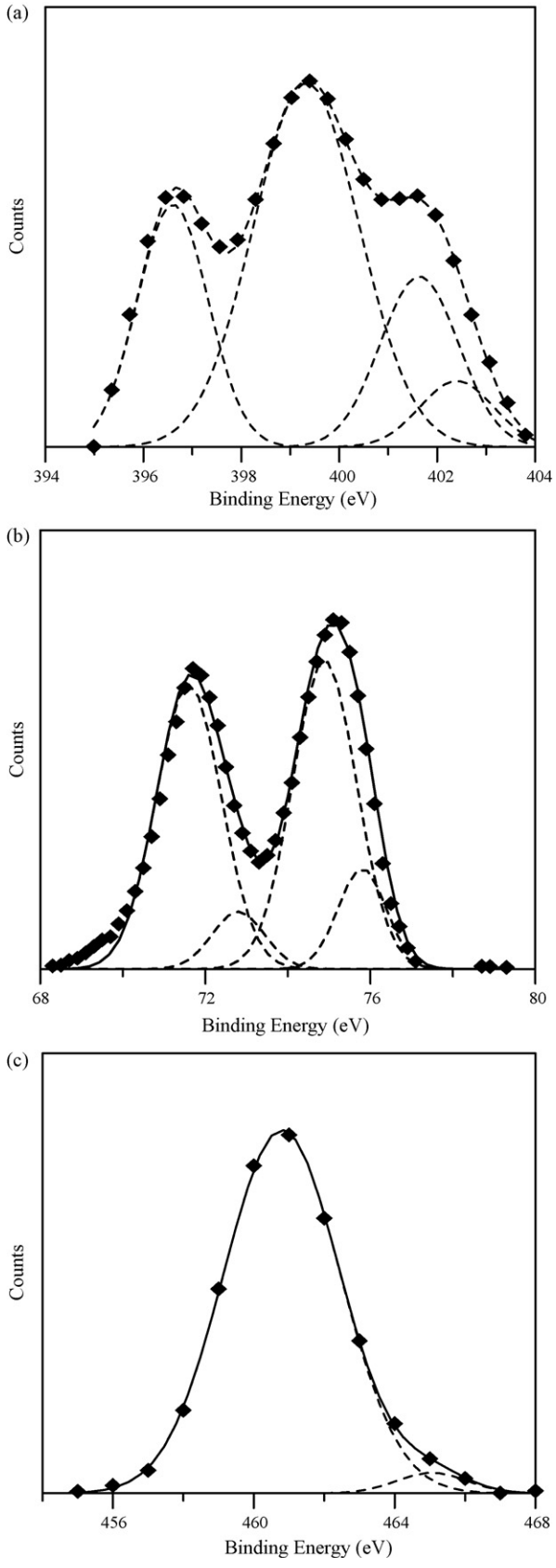

Fig. 4. (a) Nitrogen 1s, (b) platinum 4f, and (c) ruthenium 3p XPS core-level spectra of the PDMA–PSS–Pt–Ru nanocomposite.

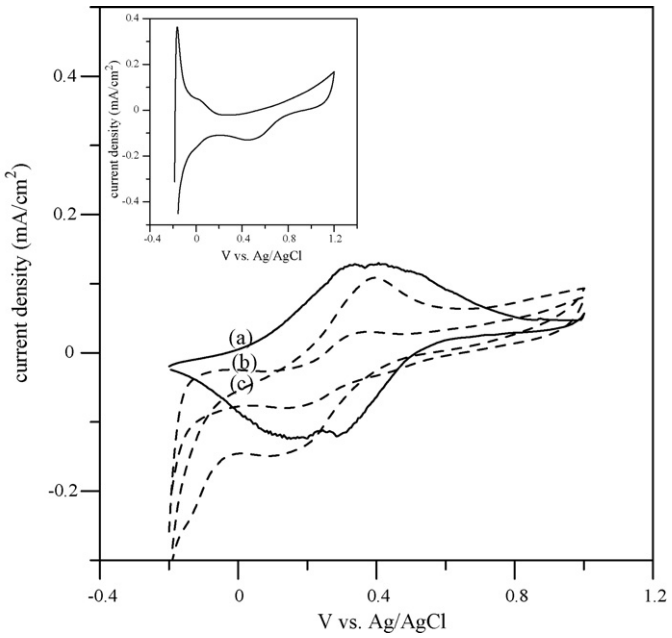

Fig. 5. Cyclic voltammograms of (a) PDMA–PSS, (b) PDMA–PSS–Pt, and (c) the PDMA–PSS–Pt–Ru nanocomposite in 0.5 M H_2SO_4 at a scan rate = 5 mV s^{-1}. The inset is bulk Pt.

voluted into two binding energies of 460.8 and 465.06 eV arising, respectively, from metallic Ru (Ru(0)) and RuO_2 (Ru(IV)). From the calculation of peak areas, we found that the Ru surface species consists mainly of metallic Ru of 96.7% with a small amount (ca. 3.3%) of RuO_2. The small amount of RuO_2 is attributed to the possible electron transfer reaction between Ru and Pt within the alloy. Since the respective electronegative values of ruthenium and platinum metals are 2.11 and 2.22 in a Pt–Ru alloy, Pt and Ru will interact with each other through their d electron orbits such that there are electrons transferring from the more electropositive Ru atoms to the neighboring Pt atoms, leading to a higher Pt particle density. Interatomic charge transfer within the broad s bands is much weaker. The maximum charge donated from a Ru atom to its neighboring Pt atoms occurs where the Ru atoms have only Pt atoms as neighbors; the maximum charge acceptance by a Pt atom occurs where the Pt atoms have only Ru atoms as neighbors, influencing the polarization of the Pt–Ru in the alloy. Since the oxygen transfer requires an open oxy-hydroxide structure with abundant free Ru–OH bonds [36], such a transfer could be better realized on Ru(IV) (formation of RuO_2) than on Ru(VI) species. This observation is also supported by TEM and XRD results. Strong interactions between Pt and Ru may be responsible for the size reduction of the particles.

3.2. Electrocatalytic evaluation of bulk Pt, PDMA–PSS–Pt, and PDMA–PSS–Pt–Ru electrodes for methanol oxidation

The catalytic activities of PDMA–PSS–Pt and PDMA–PSS–Pt–Ru electrodes were evaluated and compared to that of a bulk Pt electrode (instead of using non-adherent ITO/Pt electrode). Prior to methanol oxidation, CVs in 0.5 M H_2SO_4 (Fig. 5) were measured to characterize the electrodes. Two redox pairs were observed for PDMA–PSS (curve a) due to the conversion of leucoemeraldine to emeraldine and to the emeraldine–pernigraniline transition [19]. The CV curve of the bulk Pt electrode (Fig. 5, inset) agrees with that of the polycrystalline Pt electrode reported by Paulus et al. [37]. In the region between −0.2 and +0.2 V vs. Ag/AgCl, there are significant cathodic/anodic currents due to hydrogen adsorption/desorption. As can be seen in Fig. 5, PDMA–PSS–Pt

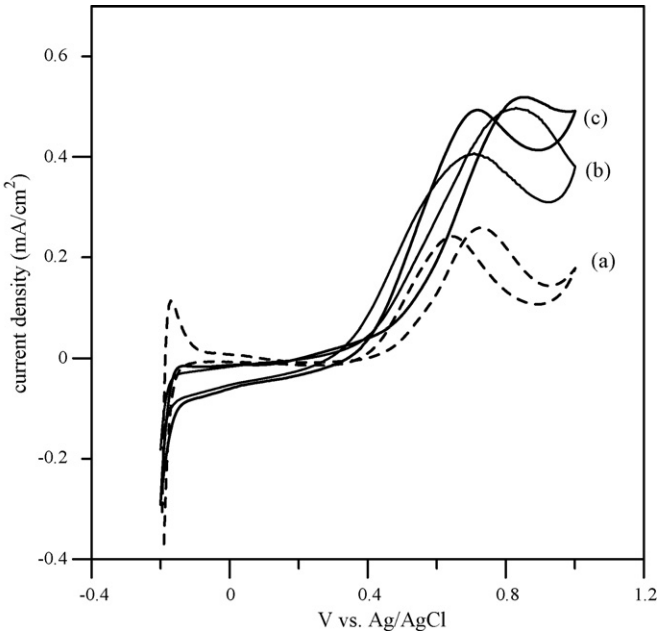

Fig. 6. Cyclic voltammograms of (a) bulk Pt, (b) PDMA–PSS–Pt, and (c) PDMA–PSS–Pt–Ru nanocomposites in 1.0 M CH_3OH + 0.5 M H_2SO_4 at the potential range of −0.2 to +1.0 V.

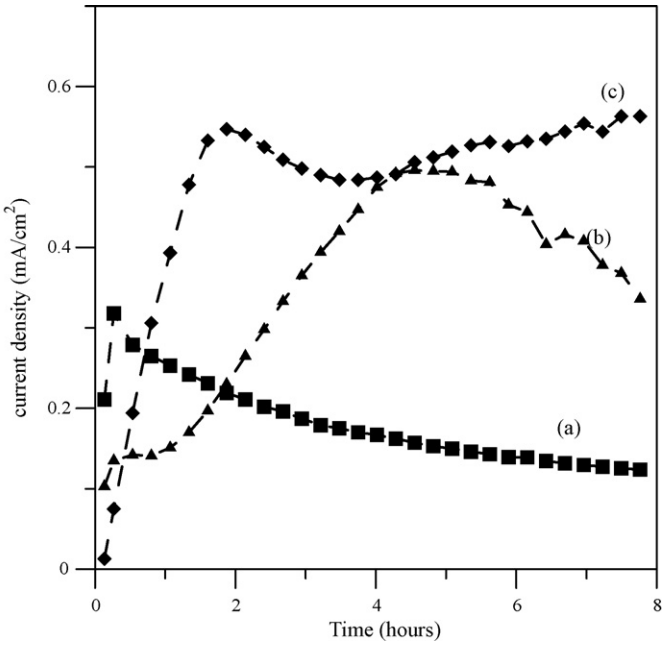

Fig. 7. Long-term stability of (a) bulk Pt, (b) PDMA–PSS–Pt, and (c) PDMA–PSS–Pt–Ru in 0.5 M H_2SO_4 and 1.0 M CH_3OH aqueous solution. *Note*: Experiment was carried out by using cyclic voltammetry bulk Pt, PDMA–PSS–Pt, and PDMA–PSS–Pt–Ru in 0.5 M H_2SO_4 and 1.0 M CH_3OH from −0.2 to 1.0 V at a scan rate as 5 mV s^{-1} for 60 cycles (8 h).The anodic current for methanol was collected at 0.85 V and operating time was estimated from cycle numbers.

(curve b) and PDMA–PSS–Pt–Ru (curve c) have similar hydrogen adsorption characteristics, indicating that Pt nanoparticles are embedded in the PDMA–PSS matrix. The disappearance of the peak corresponding to the hydrogen desorption in Fig. 5(b and c) might be attributed to the small amount of Pt content and a good dispersion in the PDMA–PSS matrix. A similar result was reported in the literature [38]. There are no Pt islands in PDMA–PSS which should have the same desorption properties as the bulk Pt. But when more Pt is deposited, the voltammograms of this PDMA–PSS–Pt/PDMA–PSS–Pt–Ru electrode look like that of a bulk Pt electrode with a hydrogen adsorption/desorption properties. It should be noted that PDMA–PSS–Pt–Ru exhibits a larger current than PDMA–PSS–Pt for hydrogen adsorption, indicating that more active sites are available to hydrogen adsorption. It is also evident that Pt–Ru nanoparticles become smaller and mono dispersive when Ru is added to the PDMA–PSS matrix, in accordance with the TEM images (Fig. 1).

The electrocatalytic activities of bulk Pt, PDMA–PSS–Pt, and PDMA–PSS–Pt–Ru towards methanol oxidation were evaluated by recording the CVs of a solution of 1.0 M CH_3OH + 0.5 M H_2SO_4 at a scanning rate of 5 mV s^{-1}, as shown in Fig. 6. Methanol oxidation commenced at about 0.4 V, yielding a peak at about 0.85 V. On the reverse scan, an oxidation peak occurred at about 0.65 V, and no reduction peak was observed. At the bulk Pt electrode, the slow increase in currents below 0.4 V on the forward scan results in the adsorption of poisonous intermediates (CO_{ads}) on Pt surfaces formed from the oxidation of small organic molecules [39,40]. The on-set potential of PDMA–Pt and PDMA–PSS–Pt for methanol oxidation was defined as the potential for the appearance of anodic current. The increase in anodic current at lower on-set potential can be observed for PDMA–PSS–Pt and PDMA–PSS–Pt–Ru than bulk Pt. The lower on-set potential of PDMA–PSS–Pt–Ru and PDMA–PSS–Pt might be due to the uniform dispersion of Pt/Pt–Ru nanoparticles in the PDMA–PSS matrix. Upon closer analysis of the on-set potential for PDMA–PSS–Pt and PDMA–PSS–Pt–Ru toward methanol oxidation, a slightly negative shift can be observed for PDMA–PSS–Pt–Ru. According to the bi-functional mechanism, the Pt sites in the Pt–Ru alloy have methanol dehydrogenation and strong chemisorption of methanol residues. Because the oxidation of methanol using PDMA–PSS–Pt–Ru catalysts occurs at a lower positive potential, the activity is better than that of bulk Pt. Furthermore, the observed anodic currents are 0.49 and 0.52 mA cm^{-2} at 0.85 V for PDMA–PSS–Pt and PDMA–PSS–Pt–Ru much higher than that (0.26 mA cm^{-2}) for bulk Pt electrode. This observation suggests that there would be more active sites available at PDMA–PSS–Pt and PDMA–PSS–Pt–Ru electrodes than at the Pt electrode [41]. The superior performance for methanol oxidation on PDMA–PSS–Pt–Ru can be attributed to two effects. (i) The active surface area of Pt–Ru electrocatalyst is more than that of a pure Pt catalyst due to the decrease in the particle size obtained by incorporating Ru into PDMA–PSS–Pt. (ii) The incorporation of Ru in PDMA–PSS–Pt facilitates the generation of oxygen-bounded species in the catalyst surface, aiding in the oxidation of CO and hence eliminating poisoning.

From the cyclic voltammograms (Fig. 6) of test electrodes, methanol oxidation commenced at approximately 0.4 V and reached its maximum current at about 0.85 V. The formation of reaction intermediates (CO) is below 0.4 V [39,40]. The long-term stabilities of PDMA–PSS–Pt, PDMA–PSS–Pt–Ru, and bulk Pt for methanol oxidation were examined in 1.0 M CH_3OH + 0.5 M H_2SO_4 solutions at a slow scanning rate (5 mV s^{-1}) for 60 cycles. The slow scan rate employed in the work allows CO to form below 0.4 V. We anticipate that the formation of CO and adsorption on Pt sites become significant with increasing cycle numbers for methanol oxidation. The drop of the maximum current is attributed to the CO poisoning of Pt active sites during the scanning in aqueous solution. The overall electrocatalytic performance of the test electrodes will be affected by deactivation due to the CO poisoning on Pt active sites. The plot of anodic current (at 0.85 V) for methanol oxidation vs. time (estimated from cycle numbers) is presented in Fig. 7. It shows that anodic current increases with increasing operation time at the initial stage for all the electrodes. With

increased operation time, methanol diffuses gradually from the bulk solution to the active Pt sites. However, PDMA–PSS–Pt and PDMA–PSS–Pt–Ru have longer activation times compared to that of bulk Pt because methanol molecules must overcome the steric hindrance in the PDMA–PSS polymeric matrix to diffuse before landing on the active Pt sites. After the activation, the anodic currents of methanol oxidation for all the electrodes first reach a maximum and then decrease. The decrease in the anodic current for methanol oxidation is attributable to the poisoning of active Pt sites by CO species produced during methanol oxidation. Interestingly, PDMA–PSS–Pt–Ru exhibited different characteristics from those of PDMA–PSS–Pt and bulk Pt. The current increases after a slight fall, implying that the active Pt sites might be regenerated during this period. This phenomenon can be explained by a bifunctional mechanism [42], as Pt provides sites for the dehydration of methanol and Ru does so for the oxidation of CO adsorbed on the Pt sites. In short, the PDMA–PSS–Pt–Ru composite is an excellent electrocatalyst for methanol oxidation.

4. Conclusions

Through a simple molecular design, Pt–Ru nanoparticles embedded in a polymer matrix comprising an electronically conductive polymer PDMA and an ionically conductive polymer PSS can be prepared via a one-step synthesis route. The generated Pt–Ru nanoparticles in PDMA–PSS were characterized by TEM images, with an averaged particle size of ca. 4 nm. XRD results reveal strong interactions between Pt and Ru nanoparticles. From XPS studies, Pt–Ru nanoparticles have the composition of Pt(0) and Ru(0) with a trace of Pt(IV) and Ru(IV) (RuO_2). The as-synthesized PDMA–PSS–Pt–Ru had the better electrocatalytic activity for methanol oxidation than PDMA–PSS–Pt and bulk Pt. This one-step method for the preparation of novel electrocatalysts, Pt–Ru nanoparticles in PDMA–PSS, could be extended for the distribution of Pt–Ru nanoparticles into any other polymeric substrate, such as Nafion, for DMFC application.

Acknowledgements

The financial support to his work by the National Science Council of Taiwan under grants 95-2211-E-006-409-MY3, NSC-96221-E-006-059, and NSC 96-2811-E-006-012 are gratefully acknowledged.

References

[1] B. Bae, B.K. Kho, T.H. Lim, I.H. Oh, S.A. Hong, H.Y. Ha, J. Power Sources 158 (2006) 1256.
[2] A. Bauer, E.L. Gyenge, C.W. Oloman, J. Power Sources 167 (2007) 281.
[3] K.T. Jeng, C.C. Chien, N.Y. Hsu, S.C. Yen, S.D. Chiou, S.H. Lin, W.M. Huang, J. Power Sources 160 (2006) 97.
[4] S. Tanaka, M. Umeda, H. Ojima, Y. Usui, O. Kimura, I. Uchida, J. Power Sources 152 (2005) 34.
[5] M. Kim, S. Hwang, J.S. Yu, J. Mater. Chem. 17 (2007) 1656.
[6] Fine particles: synthesis, characterization and mechanism of growth, in: T. Sugimuto (Ed.), Surfactant Science Series, vol. 92, Marcel Dekker, New York, 2000.
[7] J.Y. Kim, Z.G. Yang, C.C. Chang, T.I. Valdez, S.R. Narayanan, P.N. Kumta, J. Electrochem. Soc. 150 (2003) A1421.
[8] S. Music, S. Popovic, M. Maljkovic, K. Furic, A. Gajovic, J. Mater. Sci. Lett. 21 (2002) 1131.
[9] D.M.N. Rittner, T. Abraham (Eds.), Fine, Ultrafine and Nano Particles—New Technologies, Emerging Applications and New Markets, vol. III, Business Communications Co. Inc., Norwalk, CT, 2000.
[10] A.B.R. Mayer, Polym. Adv. Technol. 12 (2001) 96.
[11] M. Liu, W. Yu, H. Liu, J. Zhang, J. Colloid Interface Sci. 214 (1999) 231.
[12] C.W. Kuo, L.M. Huang, T.C. Wen, A. Gopalan, J. Power Sources 160 (2006) 65.
[13] L.M. Huang, W.R. Tang, T.C. Wen, J. Power Sources 164 (2007) 519.
[14] L. Niu, Q.H. Li, F.H. Wei, S.X. Wu, P.P. Liu, X.L. Cao, J. Electroanal. Chem. 578 (2005) 331.
[15] F.Y. Xie, Z.Q. Tian, H. Meng, P.K. Shen, J. Power Sources 141 (2005) 211.
[16] H. Thiele, H.S. von Levern, J. Colloid Sci. 20 (1965) 679.
[17] L.M. Huang, C.C. Tsai, T.C. Wen, A. Gopalan, J. Polym. Sci. Part A: Polym. Chem. 44 (2006) 3843.
[18] L.M. Huang, G.C. Huang, T.C. Wen, J. Polym. Sci. Part A: Polym. Chem. 44 (2006) 6624.
[19] L.M. Huang, T.C. Wen, A. Gopalan, Mater. Lett. 57 (2003) 1765.
[20] L.M. Huang, T.C. Wen, A. Gopalan, Synth. Met. 130 (2002) 155.
[21] L.M. Huang, T.C. Wen, A. Gopalan, Thin Solid Films 473 (2005) 300.
[22] E. Antolini, L. Giorgi, F. Cardellini, E. Passalacqua, J. Solid State Electrochem. 5 (2001) 131.
[23] K. Buga, R. Pokrop, A. Majkowska, M. Zagorska, J. Planes, F. Genound, A. Pron, J. Mater. Chem. 16 (2006) 2150.
[24] S. Shreepathi, R. Holze, Chem. Mater. 17 (2005) 4078.
[25] H.B. Xia, D.M. Cheng, C.Y. Xiao, H.S.O. Chan, J. Mater. Chem. 15 (2005) 4161.
[26] H.S. Xia, Q. Wang, Chem. Mater. 14 (2002) 2158.
[27] K.R. Reddy, K.P. Lee, A. Gopalan, M.S. Kim, A.M. Showkat, Y.C. Nho, J. Polym. Sci. Part A: Polym. Chem. 44 (2006) 3355.
[28] Y.H. Lee, G. Lee, J.H. Shim, S. Hwang, J. Kwak, K. Lee, H. Song, J.T. Park, Chem. Mater. 18 (2006) 4209.
[29] Z.L. Liu, X.Y. Ling, X.D. Su, J.Y. Lee, J. Phys. Chem. B 108 (2004) 8234.
[30] D. Chu, S. Gilman, J. Electrochem. Soc. 143 (1996) 1685.
[31] T.C. Deivaraj, J.Y. Lee, J. Power Sources 142 (2005) 43.
[32] J. Zhao, P. Wang, W. Chen, R. Liu, X. Li, Q. Nie, J. Power Sources 160 (2006) 563.
[33] Y.K. Zhou, B.L. He, W.J. Zhou, H.L. Li, J. Electrochem. Soc. 151 (2004) A1052.
[34] Z.L. Liu, X.H. Lin, J.Y. Lee, W. Zhang, M. Han, L.M. Gan, Langmuir 18 (2002) 4054.
[35] F. Grohn, G. Kim, A.J. Bauer, E.J. Amis, Macromolecules 34 (2001) 2179.
[36] A.S. Arico, P. Creti, H. Kim, R. Mantegna, N. Giordano, V. Antonucci, J. Electrochem. Soc. 143 (1996) 3950.
[37] U.A. Paulus, A. Wokaun, G.G. Scherer, T.J. Schmidt, V. Stamenkovic, N.M. Markovic, P.N. Ross, Electrochim. Acta 47 (2002) 3787.
[38] H. Laborde, J.-M. Leger, C. Lamy, J. Appl. Electrochem. 24 (1994) 219.
[39] V. Selvaraj, M. Alagar, Electrochem. Commun. 9 (2007) 1145.
[40] W.S. Li, J. Lu, J.H. Du, D.S. Lu, H.Y. Chen, H. Li, Y.M. Wu, Electrochem. Commun. 7 (2005) 406.
[41] Y.M. Wu, W.S. Li, J. Lu, J.H. Du, D.S. Lu, J.M. Fu, J. Power Sources 145 (2005) 286.
[42] T. Iwasita, Electrochim. Acta 47 (2002) 3663.